To be published in "Supernovae and Gamma Ray Bursts"
ed. M. Livio et al. (Cambridge University Press)

The Properties of Hypernovae: SNe Ic 1998bw, 1997ef, and SN IIn 1997cy

By K. NOMOTO[1,2], P.A. MAZZALI[2,3], T. NAKAMURA[1], K. IWAMOTO[4], K. MAEDA[1], T. SUZUKI[1,2], M. TURATTO[5], I.J. DANZIGER[3], F. PATAT[6]

[1]Department of Astronomy, School of Science, University of Tokyo, Tokyo, Japan
[2]Research Center for the Early Universe, School of Science, University of Tokyo, Tokyo, Japan
[3]Osservatorio Astronomico di Trieste, via G. B. Tiepolo, Trieste, Italy
[4]Department of Physics, College of Science and Technology, Nihon University, Tokyo, Japan
[5]Osservatorio Astronomico di Padova, vicolo dell'Osservatorio, Padova, Italy
[6]European Southern Observatory, Garching, Germany

We discuss the properties of the hyper-energetic Type Ic supernovae (SNe Ic) 1998bw and 1997ef and Type IIn supernova (SN IIn) 1997cy. SNe Ic 1998bw and 1997ef are characterized by their large luminosity and the very broad spectral features. Their observed properties can be explained if they are very energetic SN explosions with the kinetic energy of $E_{\rm K} \gtrsim 1 \times 10^{52}$ erg, originating probably from the core collapse of the bare C+O cores of massive stars ($\sim 30 - 40 {\rm M}_\odot$). At late times, both the light curves and the spectra suggest that the explosions may have been asymmetric; this may help us understand the claimed connection with GRB's. The Type IIn SN 1997cy is even more luminous than SN 1998bw and the light curve declines more slowly than ^{56}Co decay. We model such a light curve with circumstellar interaction, which requires the explosion energy of $\sim 5 \times 10^{52}$ erg. Because these kinetic energies of explosion are much larger than in normal core-collapse SNe, we call objects like these SNe "hypernovae". The mass of ^{56}Ni in SN 1998bw is estimated to be as large as 0.5 - 0.7 $M_\odot$ from both the maximum brightness and late time emission spectra, which suggests that the asymmetry may not be extreme.

1. Introduction

Recently, there have been an increasing number of candidates for the gamma-ray burst (GRB)/supernova (SN) connection (Woosley 1993; Paczyński 1998). The first example of such a candidate was provided by SN 1998bw. SN 1998bw was discovered in the error box of GRB980425 (Kulkarni et al. 1998), only 0.9 days after the date of the gamma-ray burst and was very possibly linked to it (Galama et al. 1998).

Early spectra were rather blue and featureless, showing some similarities with the spectra of Type Ic SNe (SNe Ic), but with one major difference (Figs. 1, 2): the absorption lines were so broad in SN 1998bw that they blended together, giving rise to broad absorption trough separated by apparent 'emission peaks' (Iwamoto et al. 1998; Patat et al. 2000; Stathakis et al. 2000). This supernova was immediately recognized to be very powerful and bright (Figs. 3, 4).

Velocities in the Si II 6355Å line are as high as $30,000$ km s^{-1}. Also, the SN was very bright for a SN Ic: the observed peak luminosity, $L \sim 1.4 \times 10^{43}$ erg s^{-1}, is almost ten times higher than that of previously known SNe Ib/Ic. Models which described the SN as the energetic explosion of a C+O core of an initially massive star could successfully fit the first 60 days of the light curve (Iwamoto et al. 1998; hereafter IMN98).

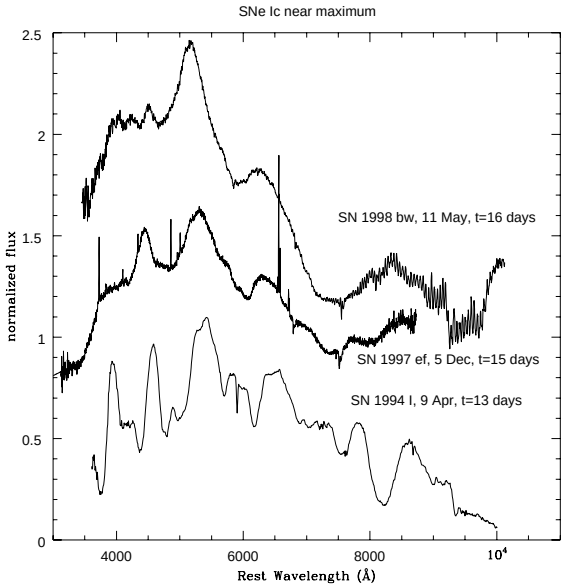

FIGURE 1. Observed spectra of Type Ic supernovae 1998bw, 1997ef, and 1994I.

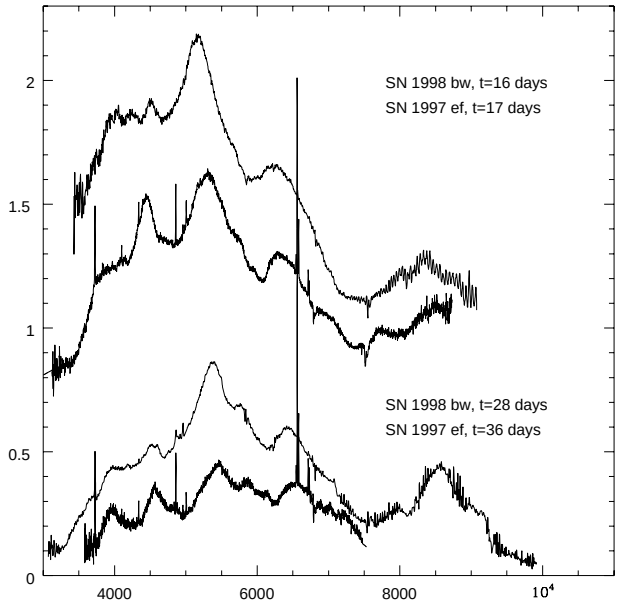

FIGURE 2. Observed spectra of Type Ic supernovae 1998bw and 1997ef.

The very broad spectral features and the light curve shape have led to the conclusion that SN 1998bw had an extremely large *kinetic* energy of explosion, $E_{\rm K} \sim 3 \times 10^{52}$ ergs (IMN98; Woosley, Eastman, & Schmidt 1999). This is more than one order of magnitude larger than the energy of typical supernovae, thus SN 1998bw was termed a "hypernova" (IMN98). "Hypernova" is a term we use to describe the events of $E_{\rm K} \gtrsim 10^{52}$ erg without specifying whether the central engine is a collapsar or magnetar or pair-instability.

SN 1997ef was also noticed for its unique light curve and spectra (Figs. 1 - 4). At

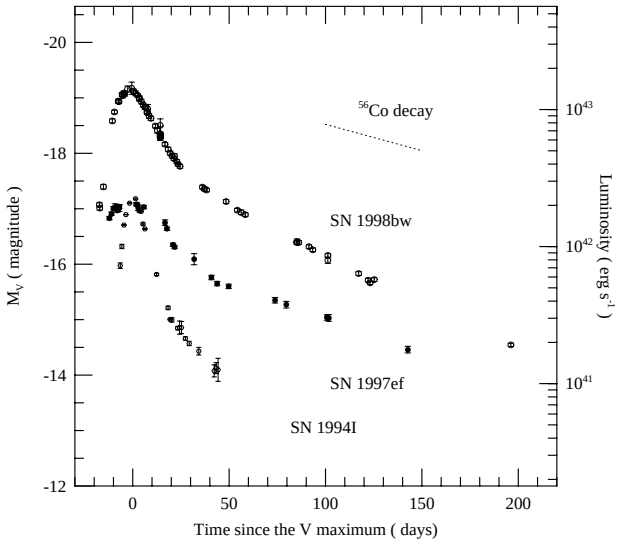

FIGURE 3. Absolute magnitudes of Type Ic supernovae: the ordinary SN Ic 1994I (Richmond et al. 1996a, b), and the hypernovae SN 1998bw (Galama et al. 1998) and SN 1997ef (Iwamoto et al. 2000). The dashed line indicates the ^{56}Co decay rate.

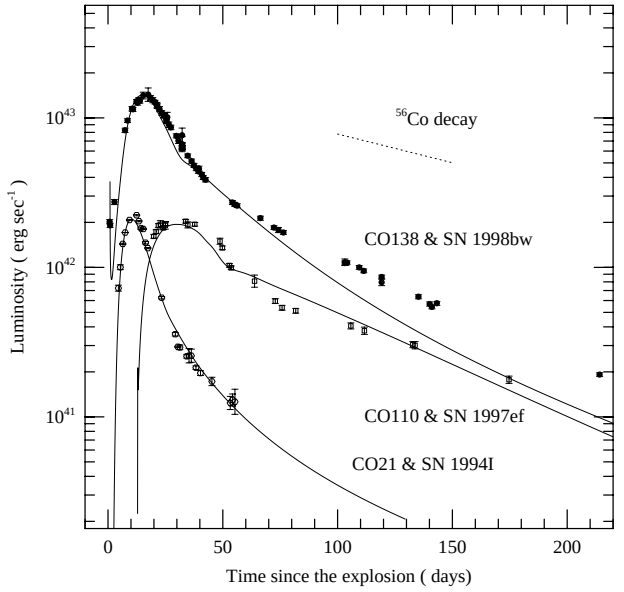

FIGURE 4. Same as Figure 3 but with theoretical models.

early times, the spectra were dominated by broad oxygen and iron absorption lines, but did not show any clear feature of hydrogen or helium (Garnavich et al. 1997a; Hu et al. 1997), which led us to classify SN 1997ef as a SN Ic. The most striking and peculiar characteristic of SN 1997ef is the width of its line features. Such broad spectral features were later recognized to be a distinguishing property of the spectra in SN 1998bw (Figs.

1, 2). The spectral similarities between SN 1997ef and SN 1998bw suggest that SN 1997ef may also be a hypernova (Iwamoto et al. 2000; Nomoto et al. 1999).

In Figure 3 the visual light curve of SNe 1998bw (Galama et al. 1998) and 1997ef (Garnavich et al. 1997b, c) are compared with the ordinary SN Ic 1994I (Richmond et al. 1996a, b). Despite the spectral similarity, the light curve of SN 1997ef is quite different from those of SN 1998bw and SN 1994I. It has a flat peak, much broader than those of the other SNe Ic. Besides, the tail of the light curve of SN 1997ef starts late and the rate of its decline is much slower than in other SNe Ic. Since the light curves are rather diverse, even in this limited number of samples, a range of energies and/or progenitor masses of SN Ic explosions may be implied.

Among the SNe with a possible GRB counterpart, we show here that the Type IIn SN 1997cy (Germany et al. 1999; Turatto et al. 1999ab) is also characterized by an extremely large kinetic explosion energy, $E_{\rm K} \gtrsim 10^{52}$ erg, thus belonging to "hypernovae". Also, SN IIn 1999E has a spectrum very similar to that of SN 1997cy (Cappellaro et al. 1999), and so it is probably a similar object.

Despite the success of our 'hypernova' model in reproducing the early light curves of SN 1998bw and SN 1997ef, the model light curve tail declines more rapidly than the observations for both SNe. Another unexpected feature appeared in the late phase spectra of SN1998bw. Measuring the velocity of each element (Patat et al. 2000), we note that iron expands faster than oxygen, which is contrary to expectations. This may indicate asymmetry in the ejecta.

Here we summarize the photometric and spectroscopic properties of these hypernovae and the estimated explosion energies and ejecta mass using the hydrodynamical models. We also study nucleosynthesis in hypernovae in 1D and 2D.

2. Explosion Models for Supernovae and Hypernovae

We construct hydrodynamical models of an ordinary SN Ic and a hypernova as follows. Since the light curve of SN Ic 1994I was successfully reproduced by the collapse-induced explosion of C+O stars (Nomoto et al. 1994; Iwamoto et al. 1994), we adopted C+O stars as progenitor models for SNe 1997ef and 1998bw as well. We calculate the light curves and spectra for various C+O star models with different values of $E_{\rm K}$ and $M_{\rm ej}$. These parameters can be constrained by comparing the calculated light curves, the synthetic spectra, and the photospheric velocities with the data of SNe 1998bw and 1997ef.

(1) In the ordinary SN Ic model (model CO60), a C+O star with a mass $M_{\rm CO} = 6.0 M_\odot$ (which is the core of a 25 $M_\odot$ main-sequence star; Nomoto & Hashimoto 1988) explodes with kinetic energy of explosion $E_{\rm K} = 1.0 \times 10^{51}$ ergs and ejecta mass $M_{\rm ej} = M_{\rm CO} - M_{\rm cut} = 4.6 M_\odot$. Here $M_{\rm cut}$ (= 1.4 $M_\odot$) denotes the mass of the compact star remnant (either a neutron star or a black hole).

(2) In the hypernova model (CO100), a C+O star of $M_{\rm CO} = 10 M_\odot$ is constructed from a 10 $M_\odot$ He star (which has a 8 $M_\odot$ C+O core) by removing the outermost 2 $M_\odot$ of He layer and extending the C+O layer up to $10 M_\odot$. This model corresponds to 30 - 35 $M_\odot$ on the main-sequence. The star explodes with $E_{\rm K} = 8.0 \times 10^{51}$ ergs, ejecting $M_{\rm ej} = 7.6 M_\odot$, i.e., $M_{\rm cut} = 2.4$ $M_\odot$.

(3) For the hypernova models CO138H and CO138L, C+O stars of $M_{\rm CO} = 13.8 M_\odot$ are constructed from a 16 $M_\odot$ He star. This model corresponds to $\sim$ 40 $M_\odot$ on the main-sequence. These models are exploded with $E_{\rm K} = 6 \times 10^{52}$ erg (CO138H) and $E_{\rm K} = 3 \times 10^{52}$ erg (CO138L) and $M_{\rm ej} \simeq 11 M_\odot$, i.e., $M_{\rm cut} \simeq 3$ - 4 $M_\odot$.

These model parameters are summarized in Table 1, together with model CO21 for SN 1994I. The position of the mass cut is chosen so that the ejected mass of ^{56}Ni is the

Table 1. Parameters of the C+O star models

model	$M_{\rm ms}(M_\odot)$	$M_{\rm C+O}$	$M_{\rm ej}$	^{56}Ni mass	$M_{\rm cut}$	$E_{\rm K}$ (10^{51} erg)	SN
CO21	~ 15	2.1	0.9	0.07	1.2	1	1994I
CO60	~ 25	6.0	4.4	0.15	1.4	1	
CO100	~ 30 - 35	10.0	7.6	0.15	2.4	8	1997ef
CO138H	~ 40	13.8	10	0.5	4	60	1998bw
CO138L	~ 40	13.8	11	0.5	3	30	1998bw

value required to explain the observed peak brightness of SN 1997ef and SN 1998bw by radioactive decay heating. The compact remnant in CO60 is probably a neutron star because $M_{\rm cut} = 1.4\ M_\odot$, while it may be a black hole in CO100 and CO138 because $M_{\rm cut}$ may well exceed the maximum mass of a stable neutron star.

The hydrodynamics at early phases was calculated by using a Lagrangian PPM code (Colella & Woodward 1984). The explosion is triggered by depositing thermal energy in a couple of zones just below the mass cut so that the final kinetic energy has the required value. The explosive nucleosynthesis are discussed in §7.

The expansion soon becomes homologous so that $v \propto r$. The solid lines in Figure 5 show the density distributions in velocity space for CO60 and CO100 at $t = 16$ days. The expansion velocities are clearly higher in CO100 than in CO60. We performed detailed radiation transfer calculations to obtain light curves and spectra for the explosion models. The results were compared with observations of SNe 1998bw and 1997ef, to derive explosion energies and the ejecta masses, and thus to determine whether the SNe were ordinary SNe Ic or hypernovae.

3. SN 1997ef

3.1. *Light Curve Models*

In Figure 6 we compare the calculated V light curves for models CO60 and CO100 with the observed V light curve of SN1997ef. We adopt a distance of 52.3 Mpc (a distance modulus of $\mu = 33.6$ mag) as estimated from the recession velocity, 3,400 km s^{-1} (Garnavich et al. 1997a) and a Hubble constant $H_0 = 65$ km s^{-1} Mpc^{-1}. We assume no color excess, $E(B-V) = 0.00$; this is justified by the fact that no signature of a narrow Na I D interstellar absorption line is visible in the spectra of SN 1997ef at any epochs (Garnavich et al. 1997a). The light curve of SN 1997ef has a very broad maximum, which lasts for ~ 25 days. The light curve tail starts only ~ 40 days after maximum, much later than in other SNe Ic.

The light curve of SN 1997ef can be reproduced basically with various explosion models with different energies and masses. In general, the properties of the light curve are characterized by the decline rate in the tail and the peak width, $\tau_{\rm peak}$. The peak width

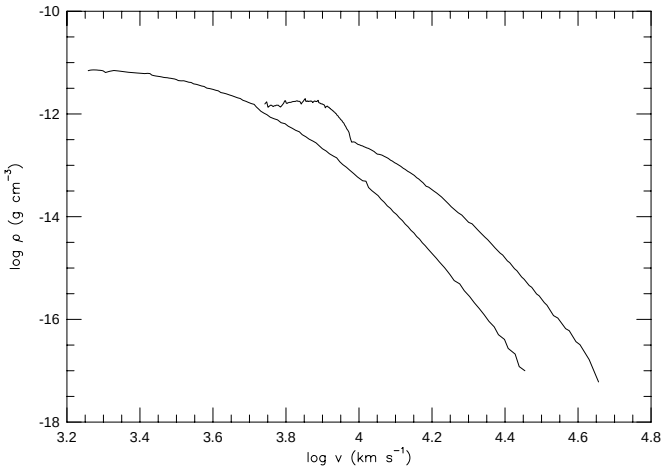

FIGURE 5. Density distributions against the vel
CO60 and C

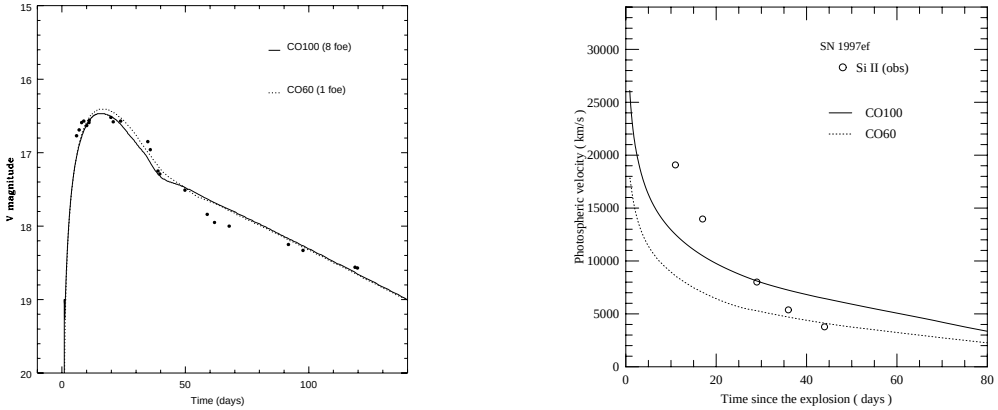

FIGURE 6. Left panel: Calculated Visual light curves of CO60 and CO100 compared with that of SN 1997ef. Right panel: Evolution of the calculated photospheric velocities of CO60 and CO100 (solid lines) compared with the observed velocities of the Si II 634.7, 637.1 nm line measured in the spectra at the absorption core.

scales approximately as

$$\tau_{\rm peak} \propto \kappa^{1/2} M_{\rm ej}^{3/4} E_{\rm K}^{-1/4}, \tag{3.1}$$

where κ denotes the optical opacity (Arnett 1996). This is the time-scale on which photon diffusion and hydrodynamical expansion become comparable. Since the model parameters of CO100 and CO60 give similar $\tau_{\rm peak}$, the light curves of the two models look similar: both have quite a broad peak and reproduce the light curve of SN1997ef reasonably well (Figure 6).

The light curve shape depends also on the distribution of ^{56}Ni, which is produced in

the deepest layers of the ejecta. More extensive mixing of ^{56}Ni leads to an earlier rise of the light curve. For SN 1997ef, the best fit is obtained when ^{56}Ni is mixed almost uniformly to the surface for both models. Without such extensive mixing, the rise time to V = 16.5 mag would be $\sim$ 30 d for CO100, which is clearly too long to be compatible with the spectroscopic dating.

Model CO60 has the same kinetic energy ($E_{\rm K} = 1 \times 10^{51}$ erg) as model CO21, which was used for SN Ic 1994I (see Table 1 for the model parameters). Since the light curve of SN 1997ef is much slower than that of SN 1994I, the ejecta mass of CO60 is $\sim$ 5 times larger than that of CO21.

The ejecta mass of CO100 is a factor of $\sim$ 2 larger than that of CO60, and it is only $\sim$ 20% smaller than that of model CO138, which was used for SN 1998bw (Table 1). Thus the explosion energy of CO100 should be $\sim$ 8 times larger than that of CO60 to reproduce the light curve of SN 1997ef. This explosion is very energetic, but still much weaker than the one in CO138. The smaller $E_{\rm K}$ for a comparable mass allows CO100 to reproduce the light curve of SN 1997ef, which has a much broader peak than that of SN 1998bw.

The light curve of SN 1997ef enters the tail around day 40. Since then, the observed V magnitude declines linearly with time at a rate of $\sim 1.1 \times 10^{-2}$ mag day^{-1}, which is slower than in other SNe Ic and is close to the ^{56}Co decay rate 9.6×10^{-3} mag day^{-1}. Such a slow decline implies much more efficient γ-ray trapping in the ejecta of SN 1997ef than in SN 1994I. The ejecta of both CO100 and CO60 are fairly massive and are able to trap a large fraction of the γ-rays, so that the calculated light curves have slower tails compared with CO21.

However, the light curves for both models decline somewhat faster in the tail than the observations. A similar discrepancy has been noted for the Type Ib supernovae (SNe Ib) 1984L and 1985F (Swartz & Wheeler 1991; Baron et al. 1993). The late time light curve decline of these SNe Ib is as slow as the ^{56}Co decay rate, so that the inferred value of M is significantly larger (and/or $E_{\rm K}$ is smaller) than those obtained by fitting the early light curve shape. Baron et al. (1993) suggested that the ejecta of these SNe Ib must be highly energetic and as massive as $\sim 50\ M_\odot$. In §4.1, we will suggest that such a discrepancy between the early- and late-time light curves might be an indication of asphericity in the ejecta of SN 1997ef and that it might be the case in those SNe Ib as well.

3.2. *Photospheric Velocities*

As we have shown, light curve modeling provides direct constraints on $M_{\rm CO}$ and $E_{\rm K}$. However, it is difficult to distinguish between the ordinary SN Ic and the hypernova model from the light curve shape alone, since models with different values of $M_{\rm ej}$ and $E_{\rm K}$ can reproduce similar light curves. However, these models are expected to show different evolutions of the photospheric velocity and the spectrum as will be discussed in the following sections.

The photospheric velocity scales roughly as $v_{\rm ph} \propto M_{\rm ej}^{-1/2} E_{\rm K}^{1/2}$, so that $M_{\rm ej}$ and $E_{\rm K}$ can be constrained by $v_{\rm ph}$ in a different way from by means of the light curve width. Figure 6 (right) shows the evolution of the observed velocities of the Si II line measured in the spectra at the absorption core, and the velocities at the grey photosphere computed by the light curve code for models CO60 and CO100. The velocities of the Si II line are somewhat higher than that of the photosphere, reaching $\sim$ 20,000 km s^{-1}at the earliest times.

In model CO60 the photosphere forms at velocities much smaller than those of the observed lines, while CO100 gives photospheric velocities as high as the observed ones.

It is clear, from this comparison, that the hyper-energetic model CO100 is preferable to the ordinary model CO60. The apparent discrepancy that still exists between the model CO100 and observations might be related to the morphology of the ejecta, i.e., a deviation from spherical symmetry, as was also suggested in the case of SN 1998bw (Höflich et al. 1999; IMN98).

3.3. *Synthetic Spectra*

To strengthen the arguments in §3.2, we compare the emergent spectra for the two explosion models. Using detailed spectrum synthesis, we can distinguish between different models more clearly, because the spectrum contains much more information than a single-band light curve.

Around maximum light, the spectra of SN 1997ef show just a few very broad features, and are quite different from those of ordinary SNe Ib/c, but similar to SN 1998bw. However, at later epochs the spectra develop features that are easy to identify, such as the Ca II IR triplet at ~ 8200Å, the O I absorption at 7500 Å, several Fe II features in the blue, and they look very similar to the spectrum of the ordinary SN Ic 1994I.

We computed synthetic spectra with a Monte Carlo spectrum synthesis code using the density structure and composition of the hydrodynamic models CO60 and CO100. The code is based on the pure scattering code described by Mazzali & Lucy (1993), but has been improved to include photon branching, so that the reprocessing of the radiation from the blue to the red is followed more accurately and efficiently (Lucy 1999; Mazzali 2000).

We produced synthetic spectra for three epochs near maximum, of SN 1997ef: Nov 29, Dec 5, and Dec 17. These are early enough that the spectra are very sensitive to changes in the kinetic energy. As in the light curve comparison, we adopted a distance modulus of $\mu = 33.6$ mag, and $E(B-V) = 0.0$.

In Figure 7 (above) we show the synthetic spectra computed with the ordinary SN Ic model CO60. The lines in the spectra computed with this model are always much narrower than the observations. This clearly indicates a lack of material at high velocity in model CO60, and suggests that the kinetic energy of this model is much too small.

Synthetic spectra obtained with the hypernova model CO100 for the same 3 epochs are shown in Figure 7 (below). The spectra show much broader lines, and are in good agreement with the observations. In particular, the blending of the Fe lines in the blue, giving rise to broad absorption troughs, is well reproduced, and so is the very broad Ca-O feature in the red. The two 'emission peaks' observed at ~ 4400 and 5200Å correspond to the only two regions in the blue that are relatively line-free.

The spectra are characterized by a low temperature, even near maximum, because the rapid expansion combined with the relatively low luminosity (from the tail of the light curve we deduce that SN 1997ef produced about $0.15 M_\odot$ of ^{56}Ni, compared to about $0.6 M_\odot$ in a typical SN Ia and $0.5 M_\odot$ in SN 1998bw) leads to rapid cooling. Thus the Si II 6355Å line is not very strong.

Although model CO100 yields rather good synthetic spectra, it still fails to reproduce the observed large width of the O I - Ca II feature in the only near-maximum spectrum that extends sufficiently far to the red (5 Dec 1997). An improvement can be obtained by introducing an arbitrary flattening of the density profile at the highest velocities.

3.4. *Possible Aspherical Effects*

We have shown that the light curve, the photospheric velocities, and the spectra of SN 1997ef are better reproduced with the hyper-energetic model CO100 than with the

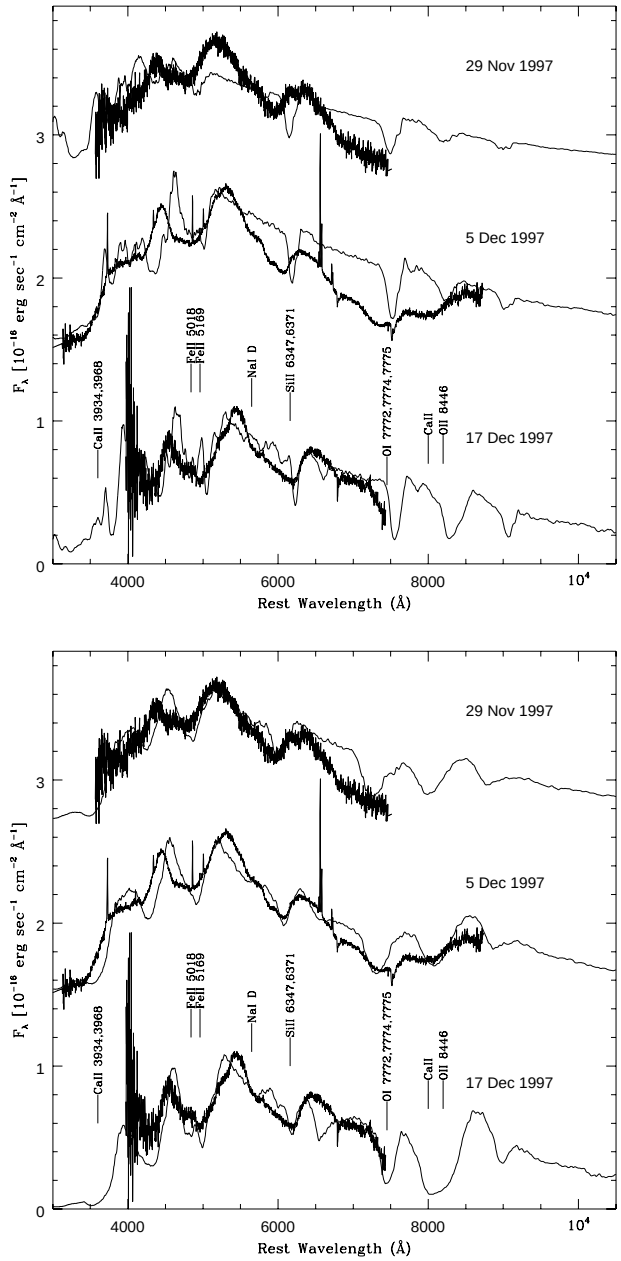

FIGURE 7. Upper panel: Observed spectra of SN 1997ef (bold lines) and synthetic spectra computed using model CO60. The lines in the synthetic spectra are much too narrow. Lower panel: Observed spectra of SN 1997ef (bold lines) and synthetic spectra computed using model CO100 (fully drawn lines).

ordinary SN Ic model CO60. However, there remain several features that are still difficult to explain with model CO100.

(1) The observed velocity of Si II decreases much more rapidly than models predict. It is as high as $\sim$ 30,000 km s^{-1} at the earliest phase, but it gets as low as $\sim$ 3,000 km s^{-1} around day 50 (Figure 6, right). We find that it is difficult to get such a rapid drop of

the photospheric velocity not only in models CO100 and CO60, but also in other models that can reproduce the light-curve shape reasonably well. Models with higher energies and/or smaller masses would be able to reproduce the fast evolution of the photospheric velocity, but such models would inevitably produce light curves with a narrower peak and a faster tail.

(2) Obviously, the observed light curve decline is slower than model CO100 in the tail part, and it is also a bit flatter than the model around maximum (Figure 6). Models with lower energies and/or larger masses give better fits to both the peak and the tail of the light curve, but then it gets very difficult to reproduce the large photospheric velocities observed at early times in SN 1997ef.

This dilemma might be overcome if we introduce multiple components of the light curve from different parts of ejecta moving at different velocities. In fact, the discrepancies may be interpreted as a possible sign of asphericity in the ejecta: A part of the ejecta moves faster than average to form the lines at high-velocities at early phases, while the other part of ejecta expands with a lower velocity so that the low-velocity Si II line comes up at later epochs. Having a low-velocity component would also make it easier to reproduce the slow tail.

(3) Extensive mixing of ^{56}Ni is required to reproduce the short rise time of the light curve. According to hydrodynamical simulations of the Rayleigh-Taylor instability in the ejecta of envelope-stripped supernovae (Hachisu et al. 1991; Iwamoto et al. 1997), large scale mixing is not expected to occur in massive progenitors, because in the core of such massive stars the density gradient is not steep enough around the composition interfaces. One possibility to induce such mixing in the velocity space is an asymmetric explosion. Higher velocity ^{56}Ni could reach the ejecta surface so that the effect of radioactive heating comes up as early as is required from light curve modeling.

In order to realize higher densities at low velocity regions without increasing the mass of the ejecta significantly, it may be necessary that the explosion is somewhat aspherical. If the explosion is aspherical, the shock would be stronger and the material would expand at a larger velocity in a certain direction, while in the perpendicular direction the shock would be weaker, ejecting lower velocity material (e.g., Höflich et al. 1999). The density of the central region could be high enough for γ-rays to be trapped even at advanced phases, thus giving rise to a slowly declining tail. In the extremely asymmetric cases, material ejection may take place in a jet-like form. A jet could easily bring some ^{56}Ni from the deepest layers out to the high velocity surface. Detailed spectral analysis of observed spectra for different epochs is necessary to investigate this issue further.

4. SN 1998bw

In this section models are presented for SN 1998bw which reproduce most of the early data. The very bright and relatively broad light curve of SN 1998bw can be reproduced by a family of models with various values of the fundamental parameters ($M_{\rm ej}$, $E_{\rm K}$), but in all the models these parameters are much larger than in the case of a typical SN Ic. All models require $M(^{56}{\rm Ni}) \sim 0.5 M_\odot$ to power the bright light curve peak. This is about an order of magnitude larger than in typical core-collapse SNe. Models with different $E_{\rm K}$ yield different synthetic spectra, and by comparing with the observed early-time spectra of SN 1998bw and trying to fit the very broad absorption features, we selected a model CO138H with $M_{\rm ej}= 10 M_\odot$, $E_{\rm K}= 6 \times 10^{52}$ erg (Nakamura et al. 1999b). The large value of $E_{\rm K}$ easily qualifies SN 1998bw as 'the' Type Ic Hypernova. The mass of the progenitor C+O star is $13.8 M_\odot$, which implies a main sequence mass of $\sim 40 M_\odot$. We also find that imposing a flatter density structure at high velocities ($v > 30,000$ km s^{-1}) results in more

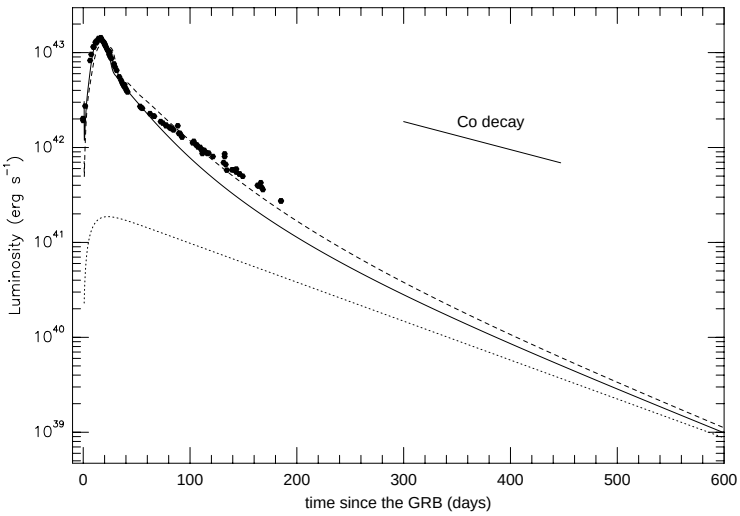

FIGURE 8. The light curves of models CO138H ($E_{\rm K} = 6 \times 10^{52}$ erg; solid) and CO138L ($E_{\rm K} = 3 \times 10^{52}$ erg; dashed) compared with the observations of SN1998bw (Galama et al. 1999; McKenzie & Schaefer 1999). A distance modulus of $\mu = 32.89$ mag and $A_V = 0.0$ are adopted. The dotted line indicates the energy deposited by positrons for CO138H.

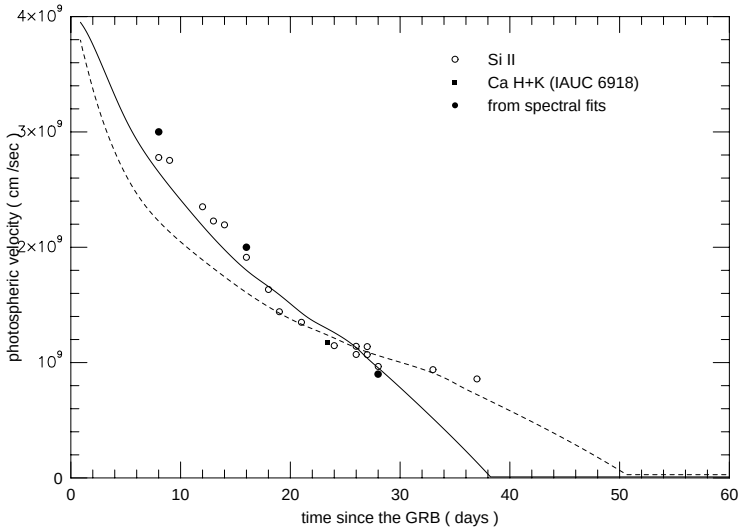

FIGURE 9. Photospheric velocities of models CO138H and CO138L compared with the observations of SN1998bw.

high-velocity absorption and in an even better-looking spectrum: significant absorption at $v \sim 60,000$ km s^{-1} is actually necessary to reproduce the observations. We then discuss the discrepancies with the later data, both light curve and spectra, and suggest that asymmetry may be playing a key role.

4.1. *Model light curves*

IMN98 modeled the SN 1998bw as the energetic explosion of a massive C+O core, and obtained a good fit to the SN light curve in the first 60 days. The model was selected from a set of degenerate models because it gave the best fit to the observed velocity of the Si II line and yielded sufficiently broad-lined spectra.

Nevertheless, the lines in the synthetic spectra were still noticeably narrower than the observed features (IMN98, Fig.2). Also, photometry after day ~ 60 show that SN 1998bw declined significantly more slowly than the rate predicted by the model. Therefore, we recompute the light curve of SN 1998bw using progenitors of different masses and explosions of different energies. All models are spherically symmetric. The ejected ^{56}Ni is assumed to be rather centrally distributed, and its mass was determined by fitting the light curve around maximum. We assume that the progenitor was a C+O star, and searched a wide range of parameters.

We find that the model that give the best agreement to both the light curve and the spectra is that of the explosion of a $13.8M_\odot$ C+O star, ejecting 10 $M_\odot$ of material with $E_{\rm K} = 6 \times 10^{52}$ erg, including $0.5M_\odot$ of ^{56}Ni (CO138H). In Figures 8 and 9 we compare the bolometric light curves and the photospheric velocities of model CO138H (solid) with the V photometry of SN 1998bw. We use $\mu = 32.97$ mag, $A_V = 0.0$ mag, and assume that $BC = 0.0$. This model has the same mass as that published in IMN98, but it has a larger $E_{\rm K}$, which is necessary to improve the fit to the spectra (§4.2).

However, CO138H has difficulties reproducing the apparently exponential decline after day 60. On the other hand, CO138L ($E_{\rm K} = 3 \times 10^{52}$; dashed) is in better agreement after day 90, although the early light curve and photospheric velocities do not fit well.

After day ~ 200 the decline of the model light curve becomes slower, and it approaches the half-life of ^{56}Co decay around day 400. At $t \gtrsim 400$ days most γ-rays escape from the ejecta, while positrons emitted from the ^{56}Co decay are mostly trapped and their energies are thermalized. Therefore, positron deposition determines the light curve at $t \gtrsim 400$ days (dotted line in Fig. 8). If the observed tail should follow the positron-powered light curve, the ^{56}Co mass could be determined directly.

The comparison between SN 1998bw and the model light curve of CO138H (which fits better at early phases) and CO138L (which is better for late phases) in Figure 8 suggests that there is a significant amount of mass expanding at very low velocity, containing some ^{56}Ni. In this case the trapping time for the γ-rays would be quite long, and the light curve might be explained. Indications for a low-velocity, high-density region are found for SN 1997ef, a lower-energy analogue of SN 1998bw.

This might indicate a departure from spherical symmetry. We will discuss this further in the next section in combination with the spectra. In any case, it is clear that the hydrodynamical model obtained from the explosion has to be altered.

4.2. *Early Time Spectra*

We have used model CO138H as a basis to compute synthetic spectra for the near-maximum phase of SN 1998bw. In particular, the model density structure and composition were used as input into the Monte Carlo code described above.

In Figure 10 we show the synthetic spectra obtained for the same 3 epochs fitted in IMN98. The observed spectra used here are the 'definitive', fully reduced version of the same ESO spectra shown in IMN98, and are calibrated with respect to the V photometry. The residual correction factors for the other bands are usually very close to 1, but they are ~ 1.1 for B in the May 11 and 23 spectra. Therefore, the new models have somewhat different parameters than those of IMN98. Both the luminosity and the photospheric velocity have increased somewhat. The photospheric velocity now is in even better agreement with the measured velocity of the Si II line (IMN98, Fig.3). All spectra are computed assuming $\mu = 32.97$ mag and $A_V = 0.0$. The assumption of zero reddening is supported by the upper limit of 0.1 Å in the equivalent width (EW) of the Na I D line obtained from high-resolution spectra (Patat et al. 2000).

The synthetic spectra clearly improve over those of IMN98. In particular, those ab-

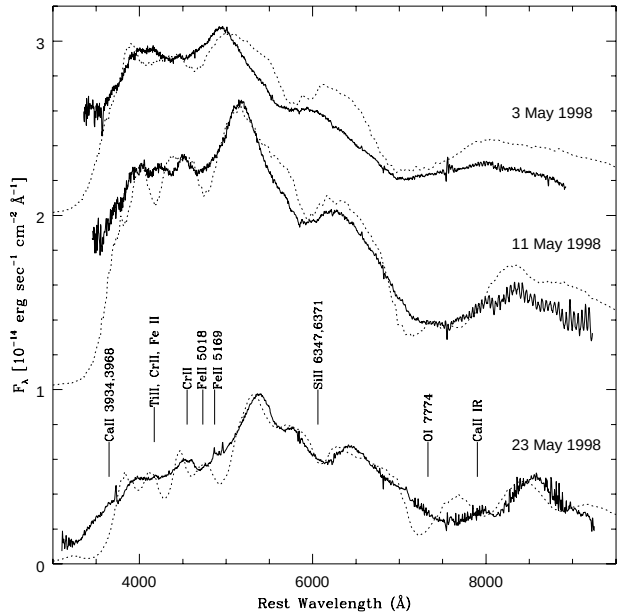

FIGURE 10. Observed spectra of SN1998bw (full lines) and synthetic spectra calculated using model CO138H ($E_{\rm K} = 6 \times 10^{52}$ erg; dashed lines).

sorptions not due to broad blends, i.e. the Si II feature near 6000Å, and the O I+Ca II feature between 7000 and 8000Å are now much broader, in significantly better agreement with the data. Nevertheless, the blue sides of those absorptions are still too narrow, indicating that even the new model may not contain enough mass at the highest velocities. Therefore we introduced an arbitrary change to the original CO138 density structure. Several possibilities were tested, and satisfactory results were found when the density slope was reduced from $\rho \propto r^{-8}$ to $\rho \propto r^{-6}$ at $v > 30,000$ km s^{-1}. This does not introduce a significant change in $M_{\rm ej}$, and increases $E_{\rm K}$ by only about 10%, but it does increase the density at high velocities, leading to significant absorption at $v \sim 60,000$ km s^{-1}in the strongest lines, especially the Ca II IR triplet, extending the absorption troughs to the blue. The corresponding synthetic spectra are shown as the dotted lines in Figure 10. The effect of the change is largest at the earliest epochs. The overall agreement with the observed spectra is better, although several problems remain, the most severe of which is clearly the excessive strength of the O I line at 7200Å on May 11 and 23. The composition is dominated by O, and it is difficult to make that line become weaker. On 23 May, the synthetic Ca II IR triplet matches the weak feature at 8000Å, which is first seen on 11 May and which continues to grow until it finally causes the wavelength of the absorption minimum of the entire broad feature to shift to $\sim$ 8200Å (Patat et al. 2000). This is rather a peculiar behavior, because on 3 May the O I and Ca II lines had to blend much more to give rise to the observed broad feature, which then had a minimum at 7000Å.

A very flat ($\rho \propto r^{-2}$) density distribution was also used by Branch (2000) to fit the spectrum of SN 1998bw. This dependence is however too flat when we use our MC model, because the ionization of e.g. Ca II does not fall as steeply as assumed by Branch (2000). On the other hand, Branch's $E_{\rm K}$ (5×10^{52} erg) is similar to ours, but he quotes a mass of $6M_\odot$ above 7000 km s^{-1}, while in our case the mass above that velocity is as large as $\sim 10M_\odot$.

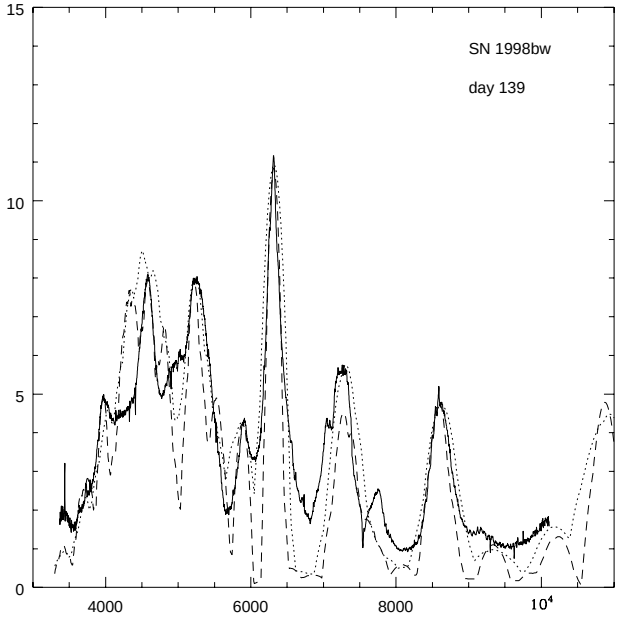

FIGURE 11. A nebular spectrum of SN 1998bw on 12 Sept 1998 (rest frame epoch 139 days) is compared to synthetic spectra obtained with a NLTE nebular model based on the deposition of gamma-rays from ^{56}Co decay in a nebula of uniform density. Two models were computed. In one model (dotted line) we tried to reproduce the broad FeII] lines near 5300Å. The ^{56}Ni mass is 0.65 $M_\odot$, and the outer nebular velocity is 11,000km s^{-1}, and the O mass is 3.5$M_\odot$. The average electron density in the nebula is log n_e = 7.47 cm^{-3}. In the other model (dashed line), we tried to reproduce only the narrow [OI] 6300Å emission line. These model has smaller ^{56}Ni mass (0.35 $M_\odot$) and O mass (2.1 $M_\odot$), and an outer velocity of 7500km s^{-1}. The density is similar to that of the 'broad-lined' model. The filling factor used is 0.1 for both models.

Clearly, a definitive solution has not been found yet. It is quite possible that only by taking into account departures from spherical symmetry it will be possible to get a really accurate fit to the spectra. Nevertheless, considering the complexity of the problem, our fits at least demonstrate that a large $E_{\rm K}$ is necessary, and that a Type Ic SN O-dominated composition yields quite a reasonable reproduction of the observations.

4.3. *Late Time Evolution*

Thus far we have presented the results of an analysis of SN 1998bw based on the spherically symmetric model CO138H, which explain the observations around the maximum. However, peculiarities in the spectrum began to appear soon after maximum, when the broad feature in the red appeared to show a 'double' Ca II absorption, or possibly an O I absorption at much lower velocity than predicted by the spherically symmetric models, which place O at the highest velocity.

Following the evolution of the spectra as they become nebular, we see that the SN showed a 'composite' spectrum (Fig. 11; Danziger et al. 1999; Patat et al. 2000): Fe II] lines, typical of SNe Ia, were strong, and so were lines of O I] and Mg I], which are typical of SNe Ib/c. At the same time, Fe III] lines, also typical of SNe Ia, were absent. The O I] and Mg I] lines grew stronger with time relative to the Fe II] lines, but had a narrower profile, maybe the composite of a broad and a narrow profile, which dominates more and more with time. The emergence of the narrow profiles occurs at about the same time as the light curve deviates from the model prediction of CO138H. In Fig. 11 we show how one nebular spectrum can be reproduced by two alternative models, one trying to

fit the broad lines, and the other aimed at fitting the narrower O I] line. The ^{56}Ni mass estimated from the broad-line fit is comparable to the value obtained from the light curve calculations.

We suggest that a rather large mass of O-dominated material is also present at low velocity. Spherical explosions do not allow that: they are very effective at 'emptying' the central region, and always place the unburned elements at the top of the ejecta. So we suggest that the explosion was highly asymmetric, leaving large quantities of unburned material expanding at low velocity in directions away from the axis along which most of the energy was released and ^{56}Ni synthesized. Our vantage point must have been very close to that axis, because we also detected the GRB. At early times, the fast-expanding lobes were much brighter than the rest, and so we observed the broad-lined spectra and the bright light curve. The ^{56}Ni mass estimate of $\sim 0.6 M_\odot$ should not change much if the explosion was not spherical. The fast-moving regions rapidly became thin, though, and soon emission lines appeared. Initially those were broad, dominated by the hyper-energetic lobes. Later, though, the γ-rays from the fast-moving ^{56}Co could escape that region more and more easily, and a significant fraction of them could penetrate down into the low-velocity region and excite the O and Mg there. Some ^{56}Ni may also be present in the low-velocity region, but that could only be determined with better S/N observations of the nebular spectrum, which require 8m-class telescopes at this point. Additional γ-ray deposition in the low-velocity region may in turn increase the deposition function above what our spherically symmetric model estimates, and thus explain the slowly declining tail of the light curve.

Both the need for a high density region and the velocity inversion as well as polarization measurements (Patat et al. 2000) might indicate that the explosion is aspherical. If the outburst in SN 1998bw took the form of a prolate spheroid, for example, the explosive shock along the long axis was probably strong, ejecting material with large velocities and producing abundant ^{56}Ni. In directions away from the long axis, on the other hand, oxygen is not much burned and the density is high enough for γ-rays to be trapped even at advanced phases, thus giving rise to the slowly declining tail.

That the SN 1998bw explosion was asymmetric is not a new suggestion: first the polarization measurements indicated an axial ratio of 2-3:1 (Höflich et al. 1999) and the calculation of the explosion of a rotating core (MacFadyen & Woosley 1999) also gave similar results, in an effort to explain the connection between SN 1998bw and GRB980425. More detailed results have to await detailed numerical models in two dimension. For the time being we can comment that if the explosion was asymmetric, most likely our results for $E_{\rm K}$ are overestimated, because those would only refer to the fast-moving part of the ejecta. As for the value of $M_{\rm ej}$, this can only be determined via 3D hydrodynamical models of the explosion, but we hope that careful analysis of the spectra, especially at late times, when both the fast and the slow components are observable, can yield at least some preliminary results.

We note that our estimate of the ^{56}Ni mass of $\sim 0.6 M_\odot$ from the nebula spectra in Figure 11 does not much depend on the asphericity. This is in good agreement with the spherical models CO138. Since Höflich et al. (1999) suggested that the ^{56}Ni mass can be as small as 0.2 $M_\odot$ if aspherical effects are large, our results suggest that the aspherical effects might be modest in SN 1998bw.

5. Type IIn SN 1997cy

SN 1997cy displayed narrow Hα emission on top of broad wings, which lead to its classification as a Type IIn (Germany et al. 1999; Turatto et al. 1999ab). Assuming

$A_V = 0.00$ for the galactic extinction (NED) we get an absolute magnitude at maximum $M_v \leq -20.1$. It is the brightest SN II discovered so far. The light curve of SN 1997cy does not conform to the classical templates of SN II, namely Plateau and Linear, but resembles the slow evolution of the Type IIn SN 1988Z. As seen from the *uvoir* bolometric light curve in Figure 12, the SN light curve decline is slower than the ^{56}Co decay rate between day 120 to 250, suggesting circumstellar interaction for the energy source. (Here the outburst is taken to be coincident with GRB970514.)

In the interaction model, collision of the SN ejecta with the slowly moving circumstellar matter (CSM) converts the kinetic energy of the ejecta into light, thus producing the observed intense light display of the SN. Our exploratory model considers the explosion of a massive star of $M = 25M_\odot$ with a parameterized kinetic energy $E_{\rm K}$. We assume that the collision starts near the stellar radius at a distance r_1, where the density of the CSM is ρ_1, and adopt for the CSM a power-law density profile $\rho \propto r^n$. The parameters $E_{\rm K}$, ρ_1, and n, are constrained from comparison with the observations.

The regions excited by the forward and reverse shock emit mostly X-rays. The density in the shocked ejecta is so high that the reverse shock is radiative and a dense cooling shell is formed (e.g., Suzuki & Nomoto 1995; Terlevich et al. 1992). The X-rays are absorbed by the outer layers and the core of the ejecta, and re-emitted as UV-optical photons.

Narrow lines are emitted from the slowly expanding unshocked CSM photoionized by the SN UV outburst or by the radiation from the shocks; intermediate width lines come from the shock-heated CSM; broad lines come from either the cooler region at the interface between ejecta and CSM.

Figure 12 shows the model light curve which best fits the observations. The model parameters are: $E_{\rm K} = 5 \times 10^{52}$ erg, $\rho_1 = 4 \times 10^{-14}$ g cm^{-3} at $r_1 = 2 \times 10^{14}$ cm (which corresponds to a mass-loss rate of $\dot{M} = 4 \times 10^{-4}\ M_\odot$ yr^{-1} for a wind velocity of 10 km s^{-1}), and $n = -1.6$. The large mass-loss episode giving rise to the dense CSM is supposed to occur after the progenitor makes a loop in the HR diagram from BSG to RSG. In this model, the mass of the low-velocity CSM is $\sim 5M_\odot$, which implies that the transition from BSG to RSG took place about 10^4 yr before the SN event.

The large CSM mass and density are necessary to have large shocked masses and thus to reproduce the observed high luminosity, and so is the very large explosion energy. For models with low $E_{\rm K}$ and high ρ_1, the reverse shock speed is too low to produce a sufficiently high luminosity. For example, a model with $E_{\rm K} = 10^{52}$ erg and ρ_1 as above yields a value of $L_{\rm UVOIR}$ lower than the observed luminosity by a factor of ~ 5. For high $E_{\rm K}$ or low ρ_1, the expansion of the SN ejecta is too fast for the cooling shell to absorb enough X-rays to sustain the luminosity. Thus in this model $E_{\rm K}$ and $\dot{M}$ are constrained within a factor of ~ 3 of the reported values.

The shape of the light curve constrains the circumstellar density structure. For $n = -2$, the case of a steady wind, $L_{\rm UVOIR}$ decreases too rapidly around day 200. To reproduce the observed decrease after day ~ 300, the CSM density is assumed to drop sharply at the radius the forward shock reaches at day 300, so that the collision becomes weaker afterwards. (Such a change of the CSM density corresponds to the transition from BSG to RSG of the progenitor $\sim 10^4$ yr before the SN explosion.) This is consistent with the simultaneous decrease in the Hα luminosity.

The observed light curve drops sharply after day 550. We reproduce such a light curve behavior (Figure 12) assuming that when the reverse shock propagates through $\sim 5\ M_\odot$, it encounters exceedingly low density region and thus it dies. In other words, the model for the progenitor of SN 1997cy assumes that most of the core material has fallen into a massive black hole of, say, $\sim 10M_\odot$, while the extended H/He envelope of $\sim 5\ M_\odot$ has

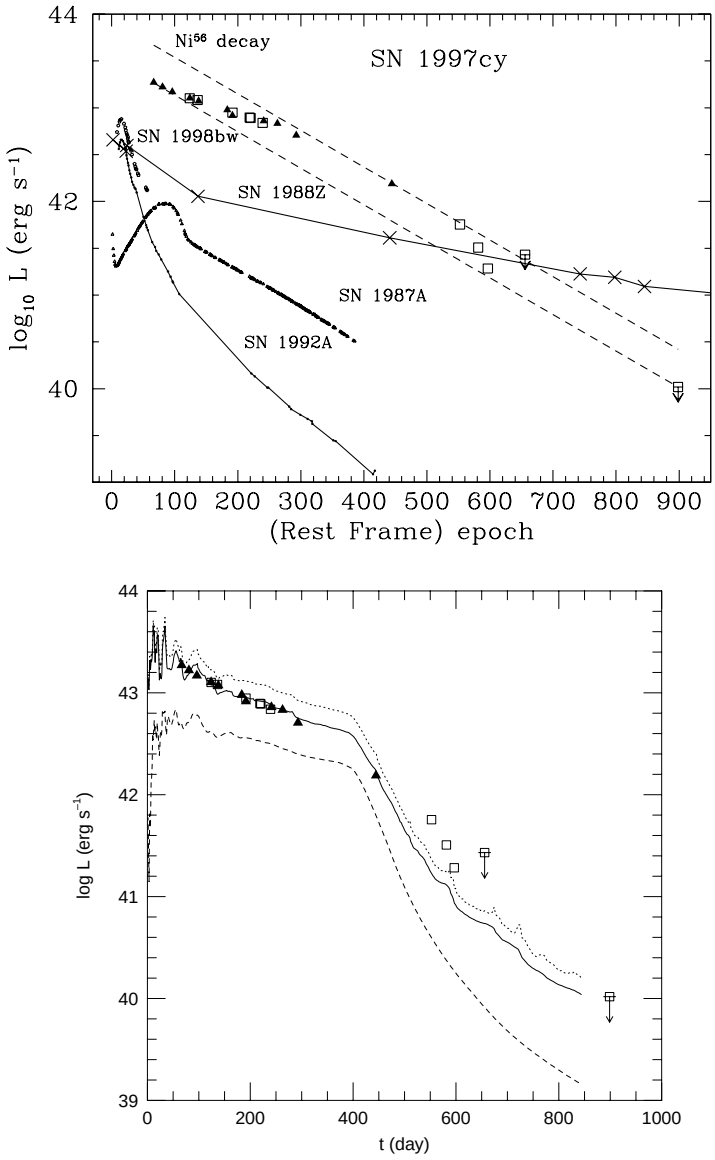

FIGURE 12. Upper panel: Observed light curves for SNe 1997cy, 1988Z, 1987A, 1992A, & 1998bw. Lower panel: The *uvoir* bolometric light curve of SN 1997cy compared with the synthetic light curve obtained with the CSM interaction model.

not collapsed. Then material is ejected from the massive black hole possibly in a jet-like form, and the envelope is hit by the "jet" and ejected at high velocity.

In this model, the ejecta are basically the H/He layers and thus contain the original (solar abundance) heavy elements plus some heavy elements mixed from the core (before fall back) or jet materials. This might explain the lack of oxygen and magnesium lines in the spectra particularly at nebular phases (Turatto et al. 1999ab).

6. Possible Evolutionary Scenarios to Hypernovae

Here we classify possible evolutionary paths leading to C+O star progenitors. In particular, we explore the paths to the progenitors that have rapidly rotating cores with a special emphasis, because the explosion energy of hypernovae may be extracted from rapidly rotating black holes (Blandford & Znajek 1977).

(1) Case of a single star: If the star is as massive as $M_{\rm ms} \gtrsim 40\ M_\odot$, it could lose its H and He envelopes in a strong stellar wind (e.g., Schaller et al. 1992). This would be a Wolf-Rayet star.

(2) Case of a close binary system: Suppose we have a close binary system with a large mass ratio. In this case, the mass transfer from star 1 to star 2 inevitably takes place in a non-conservative way, and the system experiences a common envelope phase where star 2 is spiraling into the envelope of star 1. If the spiral-in releases enough energy to remove the common envelope, we are left with a bare He star (star 1) and a main-sequence star (star 2), with a reduced separation. If the orbital energy is too small to eject the common envelope, the two stars merge to form a single star (e.g., van den Heuvel 1994).

(2-1) For the non-merging case, possible channels from the He stars to the C+O stars are as follows (Nomoto, Iwamoto, & Suzuki 1995).

(a) Small-mass He stars tend to have large radii, so that they can fill their Roche lobes more easily and lose most of their He envelope via Roche lobe overflow.

(b) On the other hand, larger-mass He stars have radii too small to fill their Roche lobes. However, such stars have large enough luminosities to drive strong winds to remove most of the He layer (e.g., Woosley, Langer, & Weaver 1995). Such a mass-losing He star would corresponds to a Wolf-Rayet star.

Thus, from the non-merging scenario, we expect two different kinds of SNe Ic, fast and slow, depending on the mass of the progenitor. SNe Ic from smaller mass progenitors (channel 2-1-a) show faster light-curve and spectral evolutions, because the ejecta become more quickly transparent to both gamma-ray and optical photons. The slow SNe Ic originate from the Wolf-Rayet progenitors (channels 1 and 2-1-b). The presence of both slow and fast SNe Ib/Ic has been noted by Clocchiatti & Wheeler (1997).

(2-2) For the merging case, the merged star has a large angular momentum, so that its collapsing core must be rotating rapidly. This would lead to the formation of a rapidly rotating black hole from which possibly a hyper-energetic jet could emerge. If the merging process is slow enough to eject the H/He envelope, the star would become a rapidly rotating C+O star. Such stars are the candidates for the progenitors of Type Ic hypernovae like SNe 1997ef and 1998bw. If a significant amount of H-rich envelope remains after merging, the rapidly rotating core would lead to a hypernova of Type IIn possibly like SN 1997cy (or Type Ib).

7. Nucleosynthesis in Hypernovae

Since hypernovae explode with much higher explosion energies than usual supernovae, explosive nucleosynthesis could have some special features. Also hypernovae have shown some aspherical signatures. Here we investigate how the explosive nucleosynthesis results depend on the explosion energy and asphericity (Nomoto et al. 1998; Nakamura et al. 1999c, 2000; Maeda et al. 2000).

7.1. *Nucleosynthesis in Spherical Explosions*

We calculate explosive nucleosynthesis in hypernovae in the same way as has been done for normal supernovae; we use a detailed nuclear reaction network including 211 isotopes up to ^{71}Ge (Thielemann, Nomoto, & Hashimoto 1996; Hix & Thielemann 1996; Nakamura

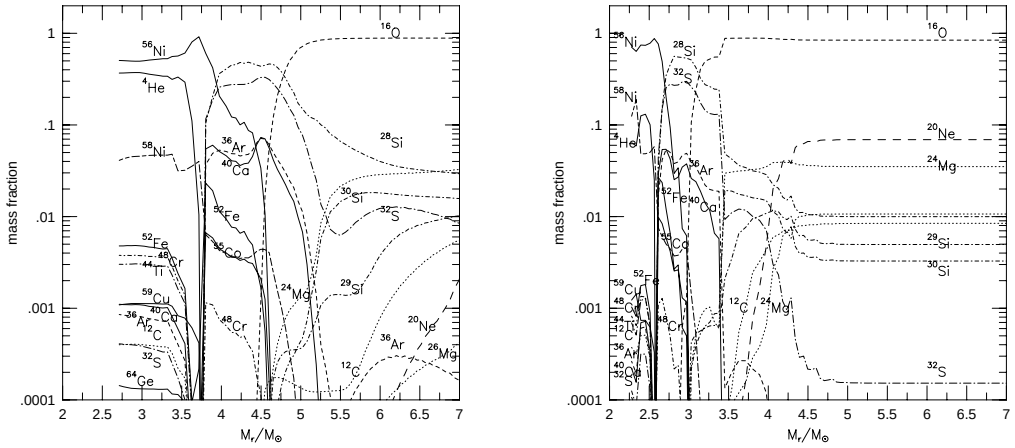

FIGURE 13. The isotopic composition of ejecta of the hypernova ($E_{\rm K} = 3 \times 10^{52}$ erg; left) and the normal supernova ($E_{\rm K} = 1 \times 10^{51}$ erg; right) for a $16 M_\odot$ He star. Only the dominant species are plotted. The explosive nucleosynthesis is calculated using a detailed nuclear reaction network including a total of 211 isotopes up to ^{71}Ge.

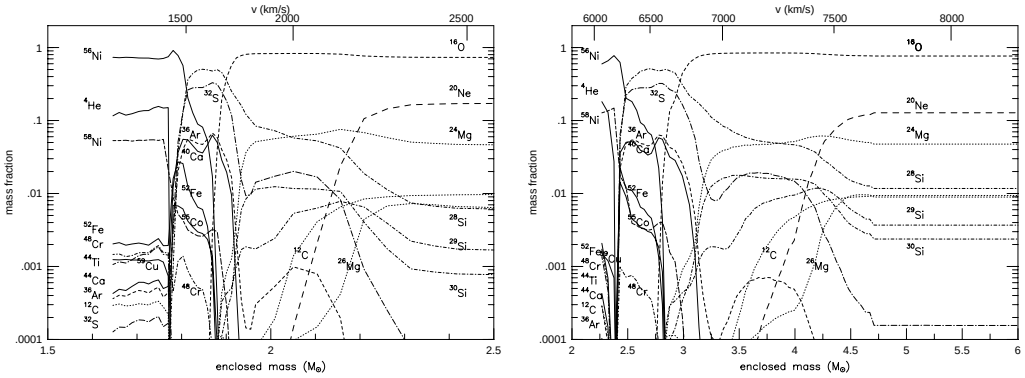

FIGURE 14. The composition structure of models CO60 (left) and CO100 (right).

et al. 1999a) (Figure 13: left). Nucleosynthesis in normal supernovae ($E_{\rm K} = 1 \times 10^{51}$ erg) is also shown in Figure 13 (right) for comparison.

A similar comparison is made in Figure 14, which shows the composition structure of models CO60 and CO100 against the expansion velocity and the Lagrangian mass coordinate of the progenitor. In CO100, the Fe and Si-rich layers expand much faster than in CO60. The total amount of nucleosynthesis products are summarized in Table 2.

From this figure, we can see the following characteristics of nucleosynthesis with the very large explosion energy.

1) The complete Si-burning region is extended to the outer, lower density region. Whether this region is ejected or not depends on the mass cut. The large amount of ^{56}Ni

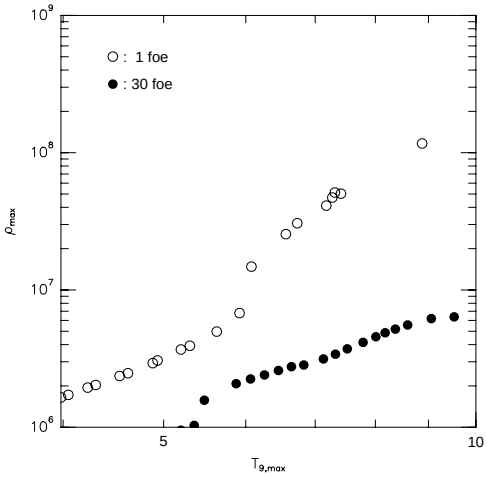

FIGURE 15. The maximum ρ - T conditions of individual mass zones in the normal supernova ($E_{\rm K}$ = 1 foe = 1×10^{51} erg) and the hypernova ($E_{\rm K}$ = 30 foe).

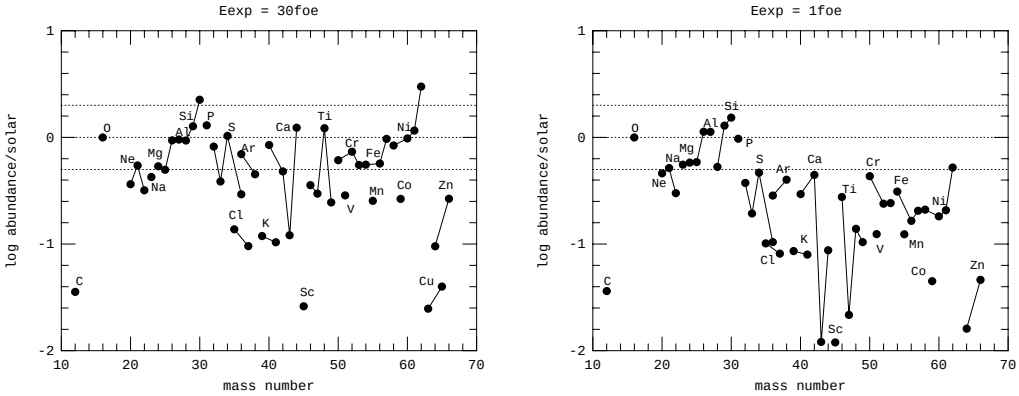

FIGURE 16. Abundances of stable isotopes relative to the solar values for 3 $\times 10^{52}$ ergs and 1 $\times 10^{51}$ ergs (Figure 13). The progenitor is a $16M_{\odot}$ He star (H-rich envelope is not included).

Table 2. Yields of hypernova and supernova models ($M_{\odot}$)

model	C	O	Ne	Mg	Si	S	Ca	Ti	Fe	Ni
CO60	0.082	3.0	0.62	0.24	0.10	0.037	0.006	0.0003	0.16	0.017
CO100	0.58	5.6	0.38	0.22	0.42	0.19	0.025	0.0003	0.19	0.021
CO138H	0.11	6.6	0.35	0.29	0.95	0.52	0.088	0.0011	0.50	0.028

model	^{44}Ti	^{56}Ni	^{57}Ni
CO60	2.1×10^{-4}	0.15	5.7×10^{-3}
CO100	4.5×10^{-5}	0.15	5.7×10^{-3}
CO138H	2.2×10^{-4}	0.50	1.5×10^{-2}

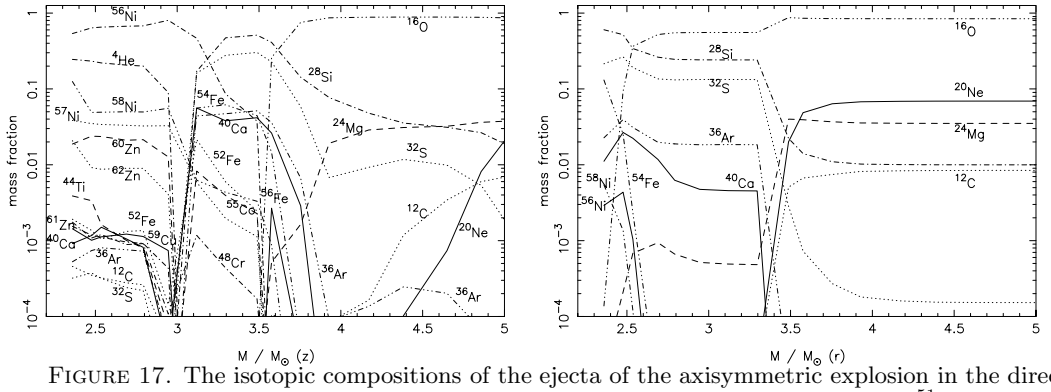

FIGURE 17. The isotopic compositions of the ejecta of the axisymmetric explosion in the direction of the jet (top) and the perpendicular to the jet (bottom) with $E_{\rm K} = 1 \times 10^{51}$ erg (Maeda et al. 2000).

observed in hypernovae (e.g., $\sim 0.5 M_\odot$ for SN1998bw and $0.15 M_\odot$ for SN1997ef) implies that the mass cut is rather deep, so that the elements synthesized in this region such as ^{59}Cu, ^{63}Zn, and ^{64}Ge (which decay into ^{59}Co, ^{63}Cu, and ^{64}Zn, respectively) are likely to be ejected more abundantly. In the complete Si-burning region of the hypernova, elements produced by α-rich freezeout are enhanced because nucleosynthesis proceeds under lower densities than in usual supernovae (Fig. 15). Figure 13 clearly shows a trend that a larger amount of ^{4}He is left in more energetic explosion. Hence, elements synthesized through α-captures such as ^{40}Ca (stable), ^{44}Ti and ^{48}Cr (decaying into ^{44}Ca and ^{48}Ti, respectively) become more abundant.

2) The more energetic explosion produces a broader incomplete Si-burning region. The elements produced mainly in this region such as ^{52}Fe, ^{55}Co, and ^{51}Mn (decaying into ^{52}Cr, ^{55}Mn, and ^{51}V, respectively) are synthesized more abundantly with the larger explosion energy.

3) Oxygen burning takes place in more extended, lower density region for the larger explosion energy, so that the abundances of elements like O, C, Al are smaller. On the other hand, a larger amount of ash products such as Si, S, Ar are synthesized by oxygen burning.

Figure 16 shows the abundances of stable isotopes relative to the solar values for 3 $\times$ 10^{52} erg and 1 $\times$ 10^{51} erg. The progenitor is the $16 M_\odot$ He star and products from H-rich envelope are not included. The isotopic ratios relative to ^{16}O with respect to the solar values are shown. As a whole, intermediate mass nuclei and heavy nuclei are more abundant for the more energetic explosion, except for the elements being consumed in oxygen burning like O, C, Al. Especially, the amounts of ^{44}Ca and ^{48}Ti are increased significantly because of the enhanced α-rich freezeout.

7.2. *Nucleosynthesis in Asymmetric Explosions*

In §4, we speculate that the expansion velocity of Fe and O in SN 1998bw betrays the effect of the asymmetry in the explosion. To confirm this we calculate the explosive nucleosynthesis in an axisymmetric explosion. Figure 17 shows the isotopic compositions of the ejecta of the axisymmetric explosion in the direction of the jet (left) and perpen-

dicular to the jet (right). The progenitor model is CO138. The the explosion energy is $E_{\rm K} = 1 \times 10^{51}$ erg. Starting the hydrodynamical simulation, we deposit the energy as 50% thermal energy and 50% kinetic energy toward the jet (z) below the mass cut that divides the ejecta and the collapsing core.

The shock is stronger and the post-shock temperatures are higher along the jet direction (z), so that explosive nucleosynthesis takes place in a more extended, lower density region compared with the perpendicular direction (r). A larger amount of ^{56}Ni is produced in the jet direction. In addition, elements produced by α-rich freezeout are enhanced because nucleosynthesis proceeds at higher entropies than in the region away from the jet. Figure 13 clearly shows that in the jet direction a larger amount of ^{4}He is left after the shock decomposition. Hence, elements synthesized through capturing α-particles such as ^{44}Ti and ^{48}Cr (decaying into ^{44}Ca and ^{48}Ti, respectively) become more abundant (see also Nagataki et al. 1997). In contrast, little ^{56}Ni is produced in the r-direction. Also the expansion velocities are lower than those in the z-direction. Therefore, the Fe velocities (mostly z-direction) can exceed the O velocities (in the r-direction), as observed in SN 1998bw. Oxygen in the z-direction has the highest velocities but the densities may become too low to be excited by gamma-rays.

Such an asymmetric ejection of nucleosynthesis products may explain the abundance features observed in X-ray Nova Sco (GRO J1655-40), which consists of a massive black hole and a low mass companion (e.g., Brandt et al. 1995; Nelemans et al. 2000). The companion star is enriched with Ti, S, Si, Mg, and O but not much Fe (Israelian et al. 1999). This is compatible with heavy element ejection from a black hole progenitor. In order to eject large amount of Ti, S, and Si and to have at least $\sim 4\ M_\odot$ below mass cut and thus form a massive black hole, the explosion should be highly energetic (Fig. 13; Israelian et al. 1999; Brown et al. 2000a; Podsiadlowski et al. 2000). Suppose that an asymmetric explosion occurred when the black hole formed in Nova Sco. Then it is likely that the companion star captured material ejected in the r-direction (i.e., on the orbital plane) which contains relatively little Fe compared with the z-direction, where burning is more effective (Podsiadlowski et al. 2000; Brown et al. 2000b). Quantitatively, nucleosynthesis in the r-direction for $E_{\rm K} = 1 \times 10^{52}$ erg is in good agreement with Nova Sco (Maeda et al. 2000).

7.3. *The Mass of Ejected ^{56}Ni*

For the study of the chemical evolution of galaxies, it is important to know the mass of ^{56}Ni, $M(^{56}\mathrm{Ni})$, synthesized in core-collapse supernovae as a function of the main-sequence mass $M_{\rm ms}$ of the progenitor star (e.g., Nakamura et al. 1999a). From our analysis of SNe 1998bw and 1997ef, we can add new points on this diagram.

We evaluate the uncertainty in our estimates of $M(^{56}\mathrm{Ni})$ and $M_{\rm ms}$. We need 0.15 $M_\odot$ of ^{56}Ni to get a reasonable fit to the light curve of SN 1997ef at a distance $D = 52.3$ Mpc. The expected 10% uncertainty in the distance leads to a 20% uncertainty in the ^{56}Ni mass, i.e., $M(^{56}\mathrm{Ni}) = 0.15 \pm 0.03\ M_\odot$. The distribution of ^{56}Ni affects the peak luminosity somewhat, but the effect is found to be much smaller than that of the uncertainty in the distance. A 10 $M_\odot$ C+O star corresponds to a $M_{\rm ms} = 30$ - 35 $M_\odot$, but the uncertainty involved in the conversion of the core mass to $M_{\rm ms}$ may involve a larger uncertainty if the progenitor undergoes close binary evolution.

Figure 18 shows $M(^{56}\mathrm{Ni})$ against $M_{\rm ms}$ obtained from fitting the optical light curves of SNe 1987A, 1993J, and 1994I (e.g., Shigeyama & Nomoto 1990; Nomoto et al. 1993, 1994; Shigeyama et al. 1994; Iwamoto et al. 1994; Woosley et al. 1994; Young, Baron, & Branch 1995). The amount of ^{56}Ni appears to increase with increasing $M_{\rm ms}$ of the progenitor, except for SN II 1997D (Turatto et al. 1998).

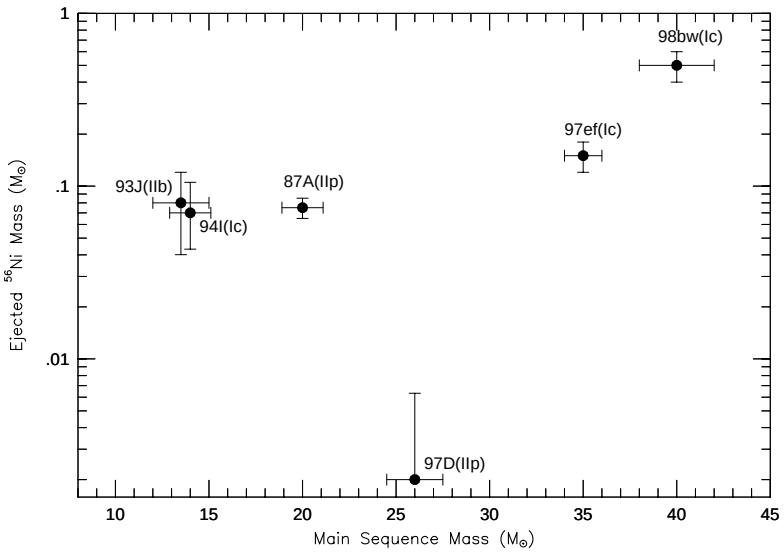

FIGURE 18. Ejected ^{56}Ni mass versus the main sequence mass of the progenitors of several bright supernovae obtained from light curve models.

This trend might be explained as follows. Stars with $M_{\rm ms} \lesssim 25\ M_\odot$ form a neutron star, producing $\sim 0.08 \pm 0.03\ M_\odot$ ^{56}Ni as in SN IIb 1993J, SN Ic 1994I, and SN 1987A (although SN 1987A may be a borderline case between neutron star and black hole formation). Stars with $M_{\rm ms} \gtrsim 25\ M_\odot$ form a black hole (e.g., Ergma & van den Heuvel 1998); whether they become hypernovae or ordinary SNe may depend on the angular momentum in the collapsing core. For SN 1997D, because of the large gravitational potential, the explosion energy was so small that most of ^{56}Ni fell back onto a compact star remnant; the fall-back might cause the collapse of the neutron star into a black hole. The core of SN II 1997D might not have a large angular momentum, because the progenitor had a massive H-rich envelope so that the angular momentum of the core might have been transported to the envelope possibly via a magnetic-field effect. Hypernovae such as SNe 1998bw, 1997ef, and 1997cy might have rapidly rotating cores owing possibly to the spiraling-in of a companion star in a binary system. The outcome certainly depends also on mass-loss rate and binarity.

8. Gamma-Ray Bursts/Supernovae Connection

Candidates for the GRB/SN connection include GRB980425/SN Ic 1998bw (Galama et al. 1998; IMN98), GRB971115/SN Ic 1997ef (Wang & Wheeler 1998), GRB970514/SN IIn 1997cy (Germany et al. 1999; Turatto et al. 1999ab), GRB980910/SN IIn 1999E (Thorsett & Hogg 1999), and GRB991002/SN IIn 1999eb (Terlevich et al. 1999).

Two other GRB's may also be associated with a SN: GRB980326 (Bloom et al. 1999) and GRB970228 (Reichart 1999; Galama et al. 1999). The optical afterglows of these GRBs showed that the decline of the light curve is slowed down at late phases, and this can be reproduced if a red-shifted SN 1998bw-like light curve is superposed on the power-law light component. A question arising from these two examples is whether the supernovae associated with GRBs have a uniform maximum luminosity, i.e., whether $\sim 0.5\ M_\odot$ ^{56}Ni production as in SN 1998bw is rather common or not. However, the present study of SN 1997ef shows that the ^{56}Ni mass and thus intrinsic maximum brightness of

SN 1997ef is smaller than in SN 1998bw by a factor of 4 - 5. We certainly need more examples for defining the luminosity function and the actual distribution of masses of ^{56}Ni produced in supernovae/hypernovae.

Among the possible connections suggested above, the statistical significance for the case of SN 1997ef and GRB971115 is much weaker than for the case of SN 1998bw and GRB980425. Recently another SN Ic, 1998ey, showed a spectrum with very broad features, very similar to that of SN1997ef on Dec 17 (Garnavich et al. 1998); but no GRB counterpart has been proposed for SN 1998ey. Although this may cast some doubt on the general association between hypernovae and GRBs, it must be noted that both SNe 1997ef and 1998ey were less energetic events than SN 1998bw. It is possible that a weaker explosion is less efficient in collimating the γ-rays to give rise to a detectable GRB (GRB980425 was already quite weak compared to the average GRBs), or that some degree of inclination of the beam axis to the line-of-sight results in a seemingly weaker supernova and in the non-detection of a GRB. Only the accumulation of more data will allow us to address these questions.

9. Concluding remarks

We have calculated the light curves and spectra for various C+O star models with different values of $E_{\rm K}$ and $M_{\rm ej}$ and reached several striking conclusions.

We have shown that the spectra of SNe 1998bw and 1997ef are much better reproduced with the hypernova models than with the ordinary SN Ic model. Since SN1998bw was connected to a highly non-spherical event like a GRB, departure from spherical symmetry could be expected. Early polarization measurements confirmed this: polarization of $\sim 1\%$, decreasing with time, was detected.

The evidence for asphericity in SN 1998bw becomes even stronger with the extended time coverage: the light curve decline is slower than predicted by our spherically symmetric model; the composite nebular spectra have different velocities in lines of different elements, with iron expanding more rapidly than oxygen; the O I] nebular line declines more slowly than the Fe II ones, signaling deposition of γ-rays in a slowly-moving O-dominated region.

The smaller line velocities at advanced phases and the flat light curve tail of SN 1997ef may also suggest the presence of a low-velocity, relatively dense core, while the high line velocities at early phases imply the presence of an even higher-velocity component of the ejecta. This discrepancy between models and observations, as well as the extensive mixing of ^{56}Ni required to explain the early rise of the light curve, seems to indicate that the explosion of SN 1997ef was at least somewhat aspherical.

Therefore, we suggest that SNe 1997ef, 1998ey, and 1998bw form a new class of hyper-energetic Type Ic supernovae, which we may call "Type Ic" hypernovae. SN 1998bw produced ~ 0.5 - $0.7 M_\odot$ of ^{56}Ni, as much as a SN Ia, while SN 1997ef produced less, only $\sim 0.15 M_\odot$, but still more than in ordinary SNe Ic. SN 1997ef also appeared to be less energetic than SN 1998bw. This may be a real difference, but it may also result from different inclination or beaming properties, since no GRB counterpart was positively observed for SN 1997ef.

SNe 1997cy, 1999E, and 1999eb may form a class of "Type IIn" hypernovae. They are also distinguished by their large kinetic energies, 8 - 60 times larger than in ordinary supernovae, but it is not easy to determine how much ^{56}Ni they produced since their light curves and spectra are dominated by interaction with a massive CSM. Simulations of the interaction can reproduce the observed light curve of SN 1997cy, indicating that

the progenitor must have been a massive star, which possibly underwent spiral-in of the companion star in a close binary system.

Continuing observations and theoretical modeling of this interesting class of objects are certainly necessary.

This work has been supported in part by the grant-in-Aid for COE Scientific Research (07CE2002) of the Ministry of Education, Science, Culture and Sports in Japan.

REFERENCES

Arnett, W.D. 1996, Supernovae and Nucleosynthesis (Princeton University Press)

Baron, E., Young, T. R., & Branch, D. 1993, ApJ, 409, 417

Branch 2000, this volume

Blandford, R. D. & Znajek, R. L. 1977, MNRAS, 179, 433

Bloom, J.S. et al. 1999, Nature, 401, 453

Brandt, W.N., Podsiadlowski, Ph., & Sigurdssen, S. 1995, MNRAS, 277, L35

Brown, G.E., Lee, C.-H., Wijers, R.A.M.J., Lee, H.K., Israelian, G., & Bethe, H.A. 2000a, preprint

Brown, G.E., Lee, C.-H., Lee, H.K., & Bethe, H.A. 2000b, in Cosmic Explosions, ed. S.S. Holt & W.W. Zhang (AIP), in press

Cappellaro, E., Turatto, M., & Mazzali, P. 1999, IAU Circ. No.7091

Clocchiatti, A., & Wheeler, J. C. 1997, ApJ, 491, 375

Colella, P., & Woodward, P. R. 1984, J. Comput. Phys., 54, 174

Danziger, I.J., et al. 1999, in The Largest Explosions Since the Big Bang: Supernovae and Gamma Ray Burst, eds. M. Livio et al. (Baltimore: STScI), 9

Ergma, E., & van den Heuvel, E.P.J. 1998, A&A, 331, L29

Galama, T.J. et al. 1998, Nature, 395, 670

Galama, T.J. et al. 1999, ApJ, submitted

Garnavich, P., Jha, S., Kirshner, R., & Challis, P. 1997a, IAU Circ. No.6778

Garnavich, P., Jha, S., Kirshner, R., Challis, P., & Balam, D. 1997b, IAU Circ. No.6786

Garnavich, P., Jha, S., Kirshner, R., & Challis, P. 1997c, IAU Circ. No.6798

Garnavich, P., Jha, S., & Kirshner, R. 1998, IAU Circ. No. 7066

Germany, L.M., Reiss, D.J., Schmidt, B.P., Stubbs, C.W., Sadler, E.M. 1999, ApJ, submitted (astro-ph/9906096)

Hachisu, I., Matsuda, T., Nomoto, K., & Shigeyama T. 1991, ApJ, 368, 27

Hix, W. R. & Thielemann, F.-K. 1996, ApJ, 460, 869

Höflich, P., Wheeler, J.C., & Wang, L. 1999, ApJ, 521, 179

Hu, J. Y. et al. 1997, IAU Circ. No. 6783

Israelian, G., Rebolo, R., Basri, G., Casares, J., & Martin, E.L. 1999, Nature, 401, 142

Iwamoto, K., Nomoto, K., Höflich, P., Yamaoka, H., Kumagai, S., & Shigeyama, T. 1994, ApJ, 437, L115

Iwamoto, K., Young, T.R., Nakasato, N., Shigeyama, T., Nomoto, K., Hachisu, I., & Saio, H. 1997, ApJ, 477, 865

Iwamoto, K., Mazzali, P.A., Nomoto, K., et al. 1998, Nature, 395, 672 (IMN98)

Iwamoto, K., Nakamura, T., Nomoto, K., Mazzali, P.A., Danziger, I.J, Garnavich, P., Kirshner, R., Jha, S., Balam, D., & Thorstensen, J., 2000, ApJ, 534, in press (astro-ph/9807060)

Kulkarni, S. R. et al. 1998, Nature, 395, 663

Lucy, L.B. 1999, A&A, in press

MacFadyen, A.I. & Woosley, S.E. 1999, ApJ 524, 262

Maeda, K., Nakamura, T., Nomoto, K., & Hachisu, I. 2000, in Origin of Matter and Evolution of Galaxies, ed. S. Kubono et al. (Singapore: World Scientific), in press

Mazzali, A. P., & Lucy, L. B. 1993, A&A, 279, 447

Mazzali, A. P. 2000, A&A, submitted

McKenzie, E.H., & Schaefer, B.E. 1999, PASP, 111, 964

Nagataki, S., Hashimoto, M., Sato, K. & Yamada, S. 1997, ApJ, 486, 1026

Nakamura, T., Umeda, H., Nomoto, K., Thielemann,F.-K., & Burrows,A. 1999a, ApJ, 517, 193

Nakamura, T., Mazzali, P.A., Nomoto, K., Iwamoto, K., & Umeda, H. 1999b, Astron. Nachrichten, 320, 363

Nakamura, T., Nomoto, K., Iwamoto, K., Umeda, H., Mazzali, P.A., & Danziger, I.J. 1999c, Memorie della Società Astronomica Italiana, in press

Nakamura, T., Maeda, K., Iwamoto, K., Suzuki, T., Nomoto, K., Mazzali, P.A., Turatto, M., Danziger, I.J., & Patat, N. 2000, in IAU Symp. 195, Highly Energetic Physical Processes and Mechanisms for Emission from Astrophysical Plasmas, ed. S. Tsuruta (PASP), in press

Nelemans, G., Tauris, T.M., & van den Heuvel, E.P.J. 2000, A&A, in press (astro-ph/9911054)

Nomoto, K., & Hashimoto, M. 1988, Phys. Rep., 163, 13

Nomoto, K., Suzuki, T., Shigeyama, T., Kumagai, S., Yamaoka, H., & Saio, H. 1993, Nature, 364, 507

Nomoto, K., Yamaoka, H., Pols, O. R., van den Heuvel, E. P. J., Iwamoto, K., Kumagai, S., & Shigeyama, T. 1994, Nature, 371, 227

Nomoto, K., Iwamoto, K., & Suzuki, T. 1995, Phys. Rep., 256, 173

Nomoto, K., Nakamura, T., Iwamoto, K., Umeda, H., & Mazzali, P.A. 1998, in Nuclei in the Cosmos V, eds. N. Prantzos (Paris: Editions Frontieres), 252

Nomoto, K., Iwamoto, K., Mazzali, P.A., & Nakamura, T. 1999, Astron. Nachrichten, 320, 265

Paczyński, B. 1998, ApJ, 494, L45

Patat, F. et al., 2000, ApJ, to be submitted

Podsiadlowski, Ph., Nomoto, K., Mazzali, P.A., & Schmidt, B. 2000, preprint

Reichart, D.E. 1999, ApJ, 521, L111

Richmond, M. W., et al. 1996a, AJ, 111, 327

Richmond, M. W., Treffers, R. R., Filippenko, A. V., & Paik, Y. 1996b, AJ, 112, 732

Schaller, G., Schaerer, D., Meynet, G., & Maeder, A. 1992, A&AS, 96, 269

Shigeyama, T., & Nomoto, K. 1990, ApJ, 360, 242

Shigeyama, T., Suzuki, T., Kumagai, S., Nomoto, K., Saio, H., Yamaoka,H. 1994, ApJ, 420, 341

Stathakis, R.A., et al. 2000, MNRAS, submitted (astro-ph/0001497)

Suzuki, T., & Nomoto, K., 1995, ApJ 455, 658

Swartz, D. A., & Wheeler, J. C. 1991, ApJ, 379, L13

Terlevich, R., Tenorio-Tagle, G., Franco, J., Melnick, J., 1992, MNRAS, 255, 713

Terlevich, R., Fabian, A., Turatto, M. 1999, IAU Circ. No. 7269

Thielemann, F.-K., Nomoto, K., & Hashimoto, M. 1996, ApJ, 460, 408

Thorsett, S.E. & Hogg, D.W. 1999, GCN Cir. No.197

Turatto, M., Mazzali, P. A., Young, T. R., Nomoto, K., Iwamoto, K., Benetti, S., Cappellaro, E., Danziger, I. J., de Mello, D. F., Phillips, M. M., Suntzeff, N. B., Clocchiatti, A., Piemonte, A., Leibundgut, B., Covarrubias, R., Maza, J., Sollerman, J., 1998, ApJ, 498, L129

Turatto, M., Mazzali, P., Suzuki, T., Young, T., Nomoto, K., Benetti, S., Cappellaro, E., Danziger, I. J., Patat, R. 1999a, in The Largest Explosions Since the Big Bang: Supernovae and Gamma Ray Burst, eds. M. Livio et al. (Baltimore: STScI), 72

Turatto, M., Suzuki, T., Mazzali, P.A., Benetti, S., Cappellaro, E., Nomoto, K., Nakamura, T., Young, T.R., Patat, F. 1999b, ApJ, submitted (astro-ph/9910324)

van den Heuvel, E. P. J. 1994, in Interacting Binaries, ed. H. Nussbaumer & A.Orr (Berlin:Springer Verlag), 263

Wang, L., & Wheeler, J. C. 1998, ApJ, 504, L87

Woosley, S. E. 1993, ApJ, 405, 273

Woosley, S. E., Eastman, R. G., & Schmidt, B.P. 1999, ApJ, 516, 788

Woosley, S. E., Eastman, R. G., Weaver, T. A., & Pinto, P. A. 1994, ApJ, 429, 300

Woosley, S. E., Langer, N., & Weaver, T. A. 1995, ApJ, 448, 315

Young, T., Baron, E., & Branch, D, 1995, ApJ, 449, L51